

# Nonlinear Zeeman behavior of $\text{Cu}^{2+}$ centers in ZnS and CdS explained by a Jahn-Teller effect

T. Telahun and U. Scherz

*Institut für Theoretische Physik, Technische Universität Berlin, Germany*

P. Thurian, R. Heitz, A. Hoffmann, and I. Broser

*Institut für Festkörperphysik, Technische Universität Berlin, Germany*

(Received 6 June 1995)

The copper defect is that transition-metal impurity in II-VI compounds for which the most complete set of information has been compiled so far experimentally and theoretically. This makes it a favored system to study the mechanisms determining the optical spectra. The interpretation of the observed  $\text{Cu}^{2+}$  transitions in ZnS and CdS crystals is made using a coupling of the electronic states to a local vibrational mode of  $E$  symmetry and a moderate Jahn-Teller effect with a Huang-Rhys factor of  $S=0.8$  for ZnS and  $S=1.1$  for CdS. We report on parameter-free calculations of the magnetic-field splitting of  $\text{Cu}^{2+}$  centers in II-VI compounds, which show a general agreement with the observed spectra. For ZnS: $\text{Cu}^{2+}$  the calculated  $g$  factors agree with the observed values, though a stronger nonlinear behavior with respect to the magnetic field had been found for some of the calculated energy levels. For CdS: $\text{Cu}^{2+}$  the nonlinear behavior of the magnetic-field splitting is also reproduced by the calculation and the  $g$  factors agree for the  ${}^2E$  excited-state doublets, whereas there are some differences for the  $g$  factors of the  ${}^2T_2$  ground-state doublets, which are due to the neglect of the  $T_2$  mode coupling in the Jahn-Teller calculation.

## I. INTRODUCTION

The optical spectra, their fine structure, and magnetic-field splitting of  $\text{Cu}^{2+}$  centers in ZnS and CdS have been studied since the pioneering work of Weakliem.<sup>1-8</sup> Optical transitions between the localized  $d$  states of the impurity ion at the cation site are characterized not only by crystal-field splitting and spin-orbit coupling, but also by electron-phonon coupling. Interpretations of these spectra, using simple models for the Jahn-Teller effect, were discussed controversially up to now, and especially the Zeeman behavior was not understood, partly because of insufficient experimental data, and partly because of restricted theoretical models. Additional high-resolution measurements of the nonlinear Zeeman splitting of the transitions of  $\text{Cu}^{2+}$  centers in II-VI compounds,<sup>9-12</sup> together with theoretical methods based on more powerful computers, give us the possibility for a better understanding of these transitions in terms of a dynamical Jahn-Teller effect. Recently a method has been developed to determine the fine-structure parameters using an evolution strategy, which was successfully applied to Ni centers in CdS crystals, and which lead to an agreement of the observed nonlinear Zeeman splitting with the parameter-free calculation.<sup>13,14</sup> The basic idea is that the fine-structure fit has to be confirmed by a calculation of the nonlinear behavior of the transition lines with respect to a magnetic field without any additional parameters, which depends sensitively on the energy levels and eigenfunctions of the fine-structure Hamiltonian. We therefore applied this method to the optical and Zeeman spectra of  $\text{Cu}^{2+}$  centers in CdS and ZnS. There are, however, a number of differences compared to the Ni impurity: First of all, an isotope shift has not been observed so far, so that the electron-phonon coupling is probably not due to a local vibrational mode of  $T_2$  symmetry of the tetrahedral symmetry group. The shift of zero-phonon

lines for different masses of the Ni isotopes is due to the coupling to a local vibrational mode which must be of  $T_2$  symmetry because the other Jahn-Teller active  $E$  mode does not move the impurity and can therefore not cause an isotope shift. The absence of an isotope effect in the case of a Cu impurity is therefore a hint that the system is coupled to an  $E$  mode. Our model is therefore based on the coupling to a local vibrational mode of  $E$  symmetry, for which we were able to take up to 14 excited energy levels into account. However, for CdS: $\text{Cu}^{2+}$  this simplification leads to some discrepancies between the calculated and observed Zeeman splitting of the  ${}^2T_2$  ground state, which might be due to the neglect of coupling to a  $T_2$  mode. It is interesting to note that an isotope effect has been observed at Cu centers in ZnO,<sup>9</sup> so that the local vibrational mode must be of  $T_2$  symmetry in this case. Second, the energy spectrum of the optical transitions of the  $\text{Cu}^{2+}$  ion in CdS and ZnS, having a  $3d^9$  electron or a one-hole configuration, results from the splitting by the crystal field and spin-orbit coupling only, but not from the Coulomb interaction of the  $d$  electrons. It is therefore not clear whether a coupling of different local vibrational modes to the excited and ground states is appropriate. Such a model has turned out to be a crucial point for the understanding of the transitions at about 1.5 eV at the Ni centers in CdS.<sup>13</sup> Third, the number of observed fine-structure lines, belonging to a particular defect, is smaller for the  $\text{Cu}^{2+}$  center, so that it is more difficult to find the correct fine-structure parameters, which had to be supplemented, on the other hand, by an additional splitting parameter for the  ${}^2E$  multiplet.

However, there are several  $\text{Cu}^{2+}$  centers known in CdS and polytypic ZnS.<sup>10,12</sup> Their fine structures are quite similar for the axially distorted centers and the idea of this paper is to give a unique theoretical description of all these centers including crystal-field theory and electron-phonon interaction. Due to all simple electronic structure of the one-hole

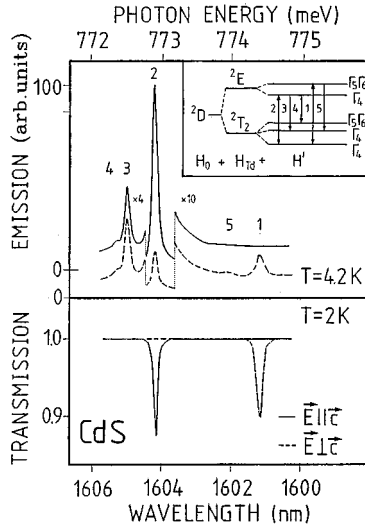


FIG. 1. Optical transitions of the  $\text{Cu}^{2+}$  center in CdS. The solid line of the emission spectrum (top) is taken at a temperature of  $T=2$  K, and the broken line at  $T=4.2$  K. The solid line of the transmission spectrum refers to a polarization parallel and the broken line perpendicular to the  $c$  axis.

system, the fine structure of the  $\text{Cu}^{2+}$  center is the ideal model system for the investigation of the Jahn-Teller effect.

## II. EXPERIMENTAL SETUP AND RESULTS

The CdS and ZnS single crystals are grown by the Broser-Warminski method,<sup>15</sup> and are subsequently doped in the ppm region by diffusion of copper. The CdS crystals are pure wurtzite crystals, whereas ZnS crystals are preferably cubic with a polytypic contribution in the order of 10–20 %. The  $\text{Cu}^{2+}$  ion substitutes the cation, and is located in a tetrahedrally coordinated  $\text{S}^{2-}$  environment in first order in both materials. In CdS and in noncubic ZnS the tetrahedron is slightly distorted, and a small trigonal distortion has to be taken into account. In the case of CdS the nearest-neighbor sulfur ion along the  $c$  axis is closer, whereas it is farther away in wurtzite ZnS compared with the other three nearest-neighbor sulfur ions.

All polytypic modifications of ZnS consist of sequences of Zn-S layers being stacked along the  $[111]_g$  direction of growth. Thus four different lattice sites exist for a substitutional impurity if the possible arrangements of the Zn-S layers above and below the two layers, which contain the impurity and their ligands, are considered. The four sites are called AN (cubic), (AS, PN) (axially distorted), and PS (hexagonal).<sup>16</sup> The letter P indicates a prismatic, A an anti-prismatic coordination, S the existence of a single third-neighbor on the stacking axis, and N its absence. In this contribution we consider six Zn-S layers, which leads to a classification scheme<sup>17</sup> of 16 different lattice sites for the substitutional  $\text{Cu}^{2+}_{\text{Zn}}$  impurity.

The tenfold degeneracy of the  ${}^2D$  multiplet of the  $\text{Cu}^{2+}$  ion, having a  $3d^9$  configuration, is lifted by a tetrahedral crystal field ( $T_d$  symmetry) into a  ${}^2T_2$  ground-state and a  ${}^2E$  excited-state multiplet. The spin-orbit interaction further splits the  ${}^2T_2$  ground state into a lower  $\Gamma_7$  doublet and a

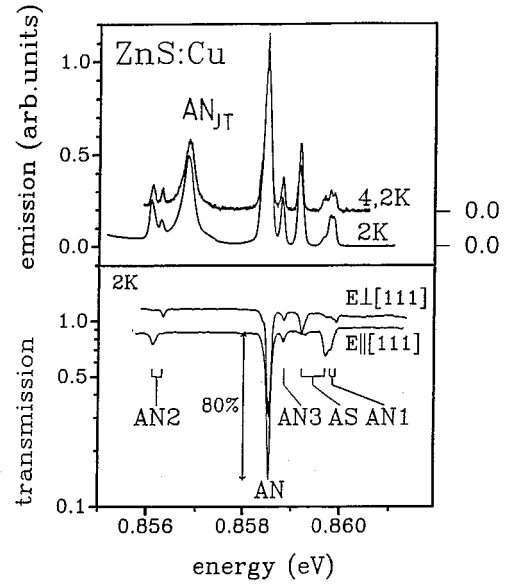


FIG. 2. Unpolarized optical transitions of  $\text{Cu}^{2+}$  centers in ZnS. The main lines AN, seen in emission (top) and transmission (bottom), are associated with the cubic centers. The other lines AN1, AN2, AN3, and AS originate from  $\text{Cu}^{2+}$  centers in different polytypes. The emission spectrum is shown at different temperatures and the transmission spectrum for polarization perpendicular and parallel to the  $c$  axis.

higher  $\Gamma_8$  quartet. The  ${}^2E$  multiplet becomes a  $\Gamma_8$  quartet of the symmetry double group. A trigonal crystal field of  $C_{3v}$  symmetry, caused by the wurtzite crystal structure or stacking faults, splits the  $\Gamma_8$  energy levels into a  $\Gamma_4$  doublet and a  $\Gamma_{56}=\Gamma_5, \Gamma_6$  Kramers doublet. The  $\Gamma_7$  state becomes a  $\Gamma_4$  state.

The high-resolution emission and absorption experiments are performed with a 0.75-m double-grating monochromator (Spex) and a cooled germanium detector (North Coast). For the luminescence experiments the crystals are excited with

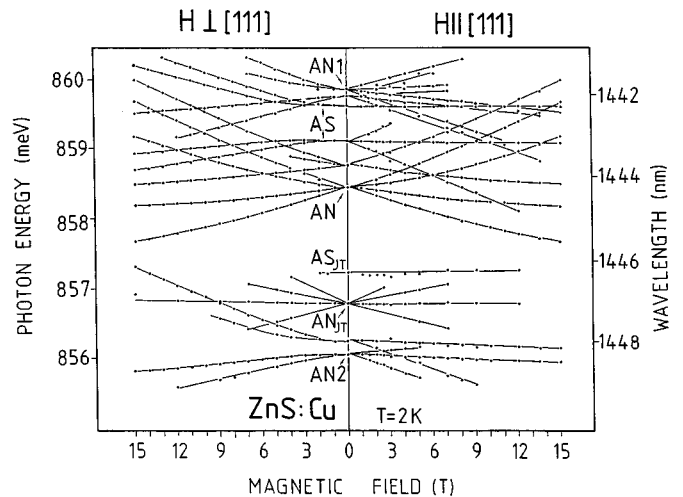


FIG. 3. Zeeman pattern of the zero-phonon lines of various  $\text{Cu}^{2+}$  centers in ZnS. The results are compiled from emission and transmission measurements.

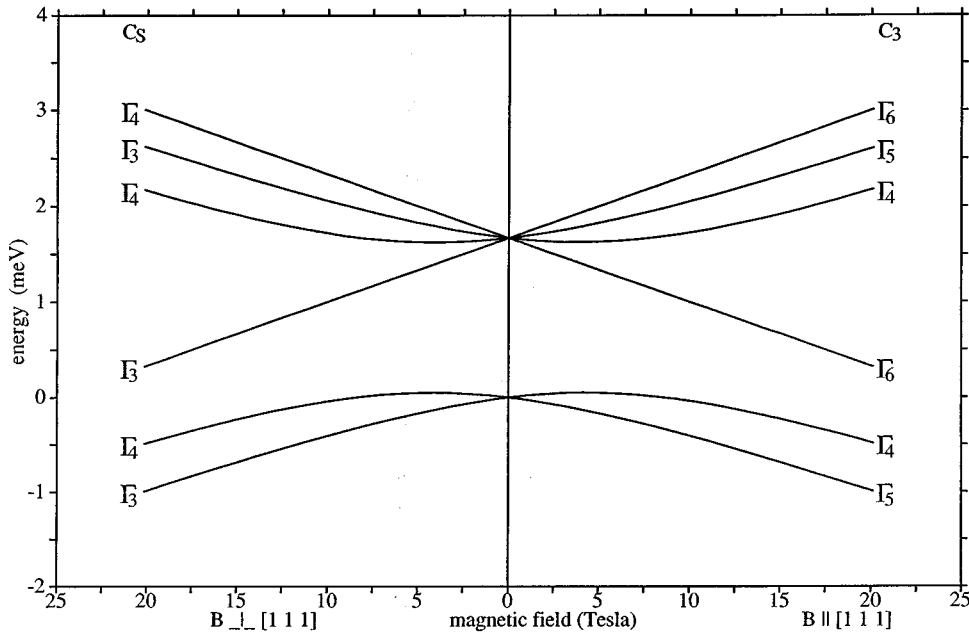


FIG. 4. Calculated magnetic-field splitting of the lowest  $\Gamma_7(^2T_2)$  and  $\Gamma_8(^2T_2)$  energy levels of the ground-state  $^2T_2$  multiplet of the cubic AN center in ZnS. The application of a magnetic field  $\mathbf{B}$  parallel or perpendicular to the [111] direction causes a reduction of the symmetry of the defect from  $T_d$  to  $C_3$  and  $C_s$ , respectively. Energies are given with respect to the zero-field  $\Gamma_7(^2T_2)$  ground state.

the blue lines of an  $\text{Ar}^+$ -ion laser in the charge-transfer band of the  $\text{Cu}^{2+}$  center. A detailed investigation of the  $\text{Cu}^{2+}$  excitation mechanism in II-VI compounds is described in Ref. 18. Here we focus our attention on the fine structure of the intracenter  $\text{Cu}^{2+}$  ( $^2E-^2T_2$ ) transition.

#### $\text{Cu}^{2+}$ in CdS

The zero-phonon line region of the  $\text{Cu}^{2+}$  emission and absorption is shown in Fig. 1. The energy differences between emission lines 2, 3, and 4 determine the threefold splitting of the  $^2T_2$  ground state. The twofold splitting of the excited  $^2E$  state is represented through the energy differences between the lines 1 and 2. Thus five Kramers doublets of the  $\text{Cu}^{2+}$  center in CdS are identified, and their relative energies listed in Table III.

#### $\text{Cu}^{2+}$ in ZnS

The region of the zero-phonon lines of the  $\text{Cu}^{2+}$  emission and absorption is shown in Fig. 2. Twelve different  $\text{Cu}^{2+}$  centers in the polymorphic ZnS crystal have been identified experimentally,<sup>9,12</sup> but here we concentrate on those for which Zeeman data are available.

#### Cubic center AN

The unpolarized zero-phonon lines of the cubic AN center are shown in Fig. 2 with high resolution. The main line, detected in emission and absorption, is attributed to the  $\Gamma_8(^2E)-\Gamma_7(^2T_2)$  transition. The unpolarized zero-phonon line at 856.78 meV is attributed to the  $\Gamma_8(^2E)-\Gamma_8(^2T_2)$  transition of the AN center.

#### Axial centers AN1, AN2, AS, and PN

The axial  $\text{Cu}^{2+}$  centers in ZnS exhibit a twofold splitting of the excited  $^2E$  state. The assignment of the different zero-phonon lines to the corresponding defect centers, and the

$^2E$  splitting, are shown in Fig. 2. We observe a zero-field splitting of 0.08; 0.20 and 0.51 meV for the AN1, AN2, and AS centers, respectively. In comparison with these axial centers the magnitude of the zero-field splitting (with respect to the magnetic field) for the PN center is increased to 2.45 meV.

It should be mentioned that the sign of the  $^2E$  splitting parameter is the same for the PN, AN1, and AN2 centers, whereas for the AS center a reversed sign is observed. The energetic positions with respect to the ground state are given in Table IV.

Thus it can be summarized that the  $^2T_2$  ground-state splitting of  $\text{Cu}^{2+}$  is strongly quenched compared to the free-ion value. This is due to covalent bonding and a Jahn-Teller effect, which is discussed in Sec. III. Furthermore, no  $^{63/65}\text{Cu}$  isotope shift has been resolved, giving us an upper limit of 10  $\mu\text{eV/nucleon}$  for  $\text{Cu}^{2+}$  in the sulfide-host compounds.

### III. THEORETICAL MODEL

The energy-level scheme of the  $\text{Cu}^{2+}$  ion in a tetrahedral and trigonal crystal field is shown in the inset of Fig. 1. In the case of the AN center there is no splitting of the excited  $^2E$  state and the higher-energy levels of the  $^2T_2$  ground state are also degenerate. This energy-level scheme of the electronic states is based on the assumption that the observed optical transitions can qualitatively be interpreted in terms of a perturbation of the energy-level scheme of the corresponding free ion. Incorporating the ion into the crystal, the ionic energy levels are split according to the symmetry of the impurity site.

Using group-theoretical arguments only, this change may be described by an effective Hamiltonian depending on a number of crystal-field parameters,<sup>19</sup>

$$H_{\text{cf}} = V(T_d) + V(C_{3v}) + H_{\text{soc}} + H_{\text{tsoc}}. \quad (1)$$

Here  $V(T_d)$  and  $V(C_{3v})$  denote the tetrahedral and trigonal crystal field, respectively,  $H_{\text{soc}}$  the spin-orbit coupling opera-

TABLE I. Fitting parameters of the optical transitions of  $\text{Cu}^{2+}$  ions in II-VI compounds. The second column gives the multiplets involved.

$Dq$	${}^2D$	tetrahedral crystal field
$D_0$	${}^2E$	higher-order trigonal spin-orbit coupling
$K$	${}^2T_2$	trigonal crystal field
$K'$	${}^2T_2, {}^2E$	trigonal crystal field
$\zeta_{\perp}$	${}^2T_2$	perpendicular spin-orbit coupling
$\zeta'_{\perp}$	${}^2T_2, {}^2E$	perpendicular spin-orbit coupling
$\zeta_{\parallel}$	${}^2T_2$	parallel spin-orbit coupling
$\zeta'_{\parallel}$	${}^2T_2, {}^2E$	parallel spin-orbit coupling
$\hbar\omega$	${}^2T_2, {}^2E$	energy of local vibrational mode
$E_{\text{JT}}=A^2/\hbar\omega$	${}^2T_2, {}^2E$	Jahn-Teller energy
$S=E_{\text{JT}}/\hbar\omega$	${}^2T_2, {}^2E$	Huang-Rhys factor

tor, and  $H_{\text{tsoc}}$  a trigonal spin-orbit coupling operator resulting from higher-order terms of perturbation theory.<sup>20</sup> The energy-level scheme is then obtained from first-order perturbation theory, and the parameters are determined by fitting to the observed spectra.

It has earlier been noted that the observed optical spectra cannot be understood using the Hamiltonian of static crystal-field theory [Eq. (1)], but must be interpreted by a dynamical Jahn-Teller effect.<sup>21,6</sup> This is done by a coupling of the electronic multiplets to a single local vibrational mode only. This simplification is possibly justified by two arguments: The probability for an optical transition at a deep impurity between vibronic states is largest for vibrational modes localized at the impurity site, and such an assumption was the basis for a successful interpretation for the fine structure of the optical transitions of  $\text{Ni}^{2+}$  impurities in CdS and the isotope shift of the lines.<sup>13</sup>

In our calculation we used a local vibrational mode of  $E$  symmetry of  $T_d$ . The reason for this is that we were able to take up to  $N=14$  excited energy levels of the local vibrational mode into account. Due to the degeneracy of the excited levels, this sums to  $(N+1)(N+2)/2$  oscillator functions in case of an  $E$  mode and to  $(N+1)(N+2)(N+3)/6$  oscillator functions in case of a  $T_2$  mode, leading to larger matrices to be diagonalized. The coupling to an  $E$  mode is

TABLE II. Fitted parameters for the  $\text{Cu}^{2+}$  centers in ZnS polytypes and CdS. AN denote the cubic and AN1, AN2, AS, and PN trigonal centers in ZnS. All parameters are given in  $\text{cm}^{-1}$ .

$\text{Cu}^{2+}$	AN	AN1	AN2	AS	PN	CdS
$N$	8	8	8	8	8	9
$Dq$	609	612	608	609	597	522
$D_0$	0	15	20	-17	128	81
$K$	0	80	81	81	80	-201
$K'$	0	11	11	11	11	-20
$\zeta_{T_d}$	-593	-589	-593	-593	-593	-559
$\zeta'_{T_d}$	-732	-732	-738	-733	-732	-618
$\zeta_{C_{3v}}$	0	65	50	-25	-58	-26
$\zeta'_{C_{3v}}$	0	65	50	-25	74	-14
$\hbar\omega$	262	261	263	264	260	272
$E_{\text{JT}}$	213	201	203	211	211	294
$S$	0.81	0.77	0.77	0.80	0.81	1.1

more likely, because it has been shown<sup>22</sup> that localized  $E$  modes with energies in the phonon energy gap between the acoustical and optical branches may exist in ZnS.

The assumptions of two different local vibrational  $E$  modes coupling independently to the  ${}^2T_2$  ground-state and the  ${}^2E$  excited-state multiplets has turned out to give less convincing results. We found that the interaction between the  ${}^2E$  and  ${}^2T_2$  multiplets is more important, especially for the Zeeman behavior. For  $\text{CdS}:\text{Cu}^{2+}$  a Zeeman splitting of the  $\Gamma_4({}^2E)$  level is observed for  $\mathbf{B} \perp \mathbf{c}$  (see Fig. 9 and Table VIII). This splitting can be explained only if the interaction between the  ${}^2E$  and  ${}^2T_2$  states is to be taken into account.<sup>9,23</sup> We therefore use the Hamiltonian

$$H = H_{\text{cf}} + H_{\text{lv}} + H_{\text{JT}} \quad (2)$$

for the first approximation of the perturbation theory. The Hamiltonian of the local vibrational mode of  $E$  symmetry and of energy  $\hbar\omega$  is given by

$$H_{\text{lv}} = \hbar\omega \sum_{k=1}^2 (a_k^+ a_k + \frac{1}{2}), \quad (3)$$

where  $a_k^+$  and  $a_k$  are creation and annihilation operators transforming as the two basis functions of the irreducible representation  $E$  of the tetrahedral symmetry group  $T_d$ . The linear Jahn-Teller coupling is described by the Hamiltonian

$$H_{\text{JT}} = A \sum_{k=1}^2 T_k (a_k^+ + a_k), \quad (4)$$

where  $T_k$  is a dimensionless electronic tensor operator transforming as  $a_k$ , and  $A$  the coupling-strength parameter. The tenfold-degenerate  ${}^2D$  multiplet is split by the tetrahedral crystal field  $V(T_d)$  in a ground-state  ${}^2T_2$  and an excited-state  ${}^2E$  multiplet. The corresponding wave functions, however, may hybridize differently with crystal  $sp$ -bonding orbitals, so that different spin-orbit coupling parameters result for the matrix elements of the  ${}^2T_2$  ground state and for matrix elements involving both multiplets.<sup>24</sup> The energy-level scheme of the Hamiltonian Eq. (2) in the case of trigonal symmetry is calculated by using the parameters compiled in Table I. In the case of cubic symmetry in ZnS, we have  $D_0 = K = K' = 0$ ,  $\zeta_{\perp} = \zeta_{\parallel}$ , and  $\zeta'_{\perp} = \zeta'_{\parallel}$ . It is therefore convenient to discuss the results in terms of tetrahedral and trigonal spin-orbit coupling parameters, defined by

$$\begin{aligned} \zeta_{T_d} &= \frac{2}{3}\zeta_{\perp} + \frac{1}{3}\zeta_{\parallel}, & \zeta_{C_{3v}} &= -\frac{1}{3}(\zeta_{\perp} - \zeta_{\parallel}), \\ \zeta'_{T_d} &= \frac{2}{3}\zeta'_{\perp} + \frac{1}{3}\zeta'_{\parallel}, & \zeta'_{C_{3v}} &= -\frac{1}{3}(\zeta'_{\perp} - \zeta'_{\parallel}). \end{aligned} \quad (5)$$

The fitting of the parameters to the observed optical transitions is complicated by the fact that the number of observed fine-structure transitions is smaller than the number of parameters shown in Table I. It is therefore difficult to find an unambiguous fit which leads to controversial interpretations.<sup>5,6,8</sup> There are, however, a number of reasonable physical limitations for the values of the parameters based on ionic properties, static crystal-field theory, and covalent bonding effects. A comparison of  $\text{Cu}^{2+}$  centers in different crystallographic environments in ZnS gives additional information about the parameters. The tetrahedral

TABLE III. Comparison of the energy levels obtained from the fitted parameters with the observed lines. The calculation took  $N=9$  excited energy levels of the local vibrational mode into account. Energies are given in meV.

CdS:Cu <sup>2+</sup>	$\Gamma_4(^2T_2)$	$\Gamma_4(^2T_2)$	$\Gamma_{56}(^2T_2)$	$\Gamma_4(^2E)$	$\Gamma_{56}(^2E)$
experiment	0.00	0.41	0.56	772.88	774.40
theory	0.00	0.39	0.47	772.88	774.41

crystal-field parameter  $Dq$  is mainly determined by static crystal-field splitting, and is expected to be the same for all the Cu<sup>2+</sup> centers. The spin-orbit coupling parameters can be estimated from the free-ion values and covalent bonding. The trigonal crystal-field parameters should be similar for different transition-metal ions in the same crystal, unless there is a considerable static Jahn-Teller displacement of the impurity, which had not been seen with these ions.<sup>8</sup> However, some differences of the trigonal crystal-field parameters are expected for the transition-metal impurities in different polytypic environments, i.e., for the PN, PS, and AS centers. The local vibrational mode energy must lie in regions of low densities of phonon states to allow for a localization at the impurity. Modes with energies in regions with large densities of phonon states hybridize with crystal phonons and thus become delocalized. This can be deduced from Raman scattering and also from model calculations of the interatomic forces. Using the valence-force model of Keating it can be shown from calculations of a large cluster of vibrating atoms around the impurity that copper centers in ZnS form local vibrational modes of  $E$  symmetry in the phonon-energy gap, whereas in CdS there are  $T_2$  modes, which are slightly split into  $A_1$  and  $E$  modes under  $C_{3v}$  symmetry.<sup>22</sup>

To start our fitting procedure we used rough estimates of the parameters as obtained from earlier fittings of static

crystal-field theory. Thus, in Ref. 2, it has been estimated that  $Dq=624$  cm<sup>-1</sup> for ZnS and  $Dq=556$  cm<sup>-1</sup> for CdS, and  $\zeta=-593$  cm<sup>-1</sup> for ZnS and  $\zeta=-565$  cm<sup>-1</sup> for CdS. The values in Ref. 21, obtained from optical spectra, are  $\zeta=-545$  cm<sup>-1</sup> for CdS and  $\zeta=-585$  cm<sup>-1</sup> for ZnS. We used these values for  $Dq$  and  $\zeta_{T_d}$  as the basis of our search. Estimates for the trigonal crystal-field parameter  $K$  have also been given in Ref. 21 by  $|K/\zeta|=0.1$ . Here we use the approximate relation  $|K/\zeta_{T_d}|\approx 0.1$  for ZnS. This relation does not hold, however, for CdS because of the approximate relation  $|K(\text{CdS})/K(\text{ZnS})|\approx 2$ , reflecting the different deviations from the ideal wurtzite lattices for CdS and ZnS.<sup>25</sup> The search for the values of  $\zeta'_{T_d}$  was based on the estimates in Ref. 20, where  $|\zeta'/\zeta|=1.44$ , and in Ref. 26 where  $|\zeta'/\zeta|=1.22$ . Thus the approximate relations  $|\zeta'_{T_d}/\zeta_{T_d}|=1.2$  and  $1.1$  for ZnS and CdS, respectively, were used here. We further adopted the relation  $|K'/K|=0.1$  for the trigonal crystal-field parameters  $K'$  for both ZnS and CdS, unlike in Ref. 20, where  $|K'/K|=1.4$ . The trigonal spin-orbit coupling parameters  $\zeta_{C_{3v}}$ ,  $\zeta'_{C_{3v}}$  are introduced by the relation  $|\zeta_{C_{3v}}/\zeta_{T_d}|=0.1$  and  $|\zeta'_{C_{3v}}/\zeta_{C_{3v}}|=1$ .

The additional splitting parameter  $D_0$  for the  $^2E$  multiplet also determines the piezoelectric behavior of this mul-

TABLE IV. Comparison between the observed and calculated (fitted) energy-level differences of Cu<sup>2+</sup> centers in ZnS. Energy levels  $\Gamma_{56}$  denote the Kramers doublet  $\Gamma_5\Gamma_6$ . In case of the cubic AN center, two calculated one-phonon lines  $\Gamma_6(^2E)$  and  $\Gamma_7(^2T_2)$  are included. Energies are given in meV.

AN ( $T_d$ )	$\Gamma_7(^2T_2)$	$\Gamma_8(^2T_2)$	$\Gamma_7(^2T_2)$	$\Gamma_8(^2E)$	$\Gamma_6(^2E)$
experiment	0.00	1.68	25.9	858.46	
theory	0.00	1.67	26.91	858.46	874.81
AN1 ( $C_{3v}$ )	$\Gamma_4(^2T_2)$	$\Gamma_{56}(^2T_2)$	$\Gamma_4(^2T_2)$	$\Gamma_4(^2E)$	$\Gamma_{56}(^2E)$
experiment	0.00			859.77	859.85
theory	0.00	1.94	2.26	859.77	859.87
AN2 ( $C_{3v}$ )	$\Gamma_4(^2T_2)$	$\Gamma_{56}(^2T_2)$	$\Gamma_4(^2T_2)$	$\Gamma_4(^2E)$	$\Gamma_{56}(^2E)$
experiment	0.00			856.07	856.27
theory	0.00	1.96	2.25	856.04	856.25
AS ( $C_{3v}$ )	$\Gamma_4(^2T_2)$	$\Gamma_{56}(^2T_2)$	$\Gamma_4(^2T_2)$	$\Gamma_{56}(^2E)$	$\Gamma_4(^2E)$
experiment	0.00	1.88		859.10	859.61
theory	0.00	1.88	2.00	859.07	859.62
PN ( $C_{3v}$ )	$\Gamma_4(^2T_2)$	$\Gamma_{56}(^2T_2)$	$\Gamma_4(^2T_2)$	$\Gamma_4(^2E)$	$\Gamma_{56}(^2E)$
experiment	0.00	1.82		844.08	846.56
theory	0.00	1.82	1.88	844.00	846.66

TABLE V. Possible splittings of the energy levels of the symmetry double groups  $T_d$  for cubic centers and  $C_{3v}$  for trigonal centers with respect to symmetry reduction for a magnetic field  $\mathbf{B}$  perpendicular or parallel to the  $[111]$  or  $c$  axis. The numbers in brackets give the dimension of the irreducible representation. The irreducible representations of the symmetry groups  $C_3$  and  $C_s$  are all one dimensional. The representation  $\Gamma_5$  and  $\Gamma_6$  of  $C_{3v}$  form a Kramers doublet.

$B \parallel [-110]$	$B=0$	$B \parallel [111]$
$C_s$	$T_d$	$C_3$
$\Gamma_3 + \Gamma_4$	$\Gamma_6(2)$	$\Gamma_4 + \Gamma_5$
$\Gamma_3 + \Gamma_4$	$\Gamma_7(2)$	$\Gamma_4 + \Gamma_5$
$2\Gamma_3 + 2\Gamma_4$	$\Gamma_8(4)$	$\Gamma_4 + \Gamma_5 + 2\Gamma_6$
$B \perp c$	$B=0$	$B \parallel c$
$C_s$	$C_{3v}$	$C_3$
$\Gamma_3 + \Gamma_4$	$\Gamma_4(2)$	$\Gamma_4 + \Gamma_5$
$\Gamma_3 + \Gamma_4$	$\Gamma_5(1) + \Gamma_6(1)$	$2\Gamma_6$

triplet of the  $\text{Cu}^{2+}$  centers in II-VI compounds. It can be deduced from the splitting of the  ${}^2E$  level, and is introduced into such a Jahn-Teller calculation for the first time, to our knowledge.

Starting with these approximate values of the parameters  $Dq$ ,  $\zeta_{T_d}$ ,  $\zeta'_{T_d}$ ,  $K$ , and  $K'$  we assumed a region of variation for any of them, and tried to reproduce the energetic positions of the observed transitions. To reduce computer time this research was done with smaller matrices taking only  $N=6$  excited energy levels of the local vibrational mode into account. This led to Huang-Rhys factors of the order of 1, corresponding to a moderate Jahn-Teller coupling. This is in agreement with the details of the phonon sidebands of the so called zero-phonon lines analyzed in Ref. 6. This set of parameters was then used to start the following fitting procedure taking more excited energy levels of the local vibrational mode into account.

At first we determined a volume in the parameter space from the approximate values, discussed above, together with a region of variation, which was typically taken to be between  $\pm 10\%$  and  $\pm 20\%$ . The search was started using equidistant points in this volume and a weighted mean-square measure to estimate the fit of differently narrow lines. The fitting was then improved with the help of an evolution strategy.<sup>13</sup> This led in all cases to one definite set of parameters with which the observed optical transitions could be

fitted. The calculations were then repeated, using up to  $N=14$  excited energy levels of the local vibrational mode, around the predetermined values. We obtained a convergence of the parameters with respect to  $N$  for  $N \geq 8$ .<sup>23</sup> This means that vibronic energy levels about 0.3 eV above the zero-phonon line could be neglected. It must be emphasized, however, that we do not claim that our fitting procedure alone leads to an unambiguous fit of the fine structure. The set of parameters must be tested by the calculation of the magnetic-field splitting without introducing additional parameters.

Our results for  $\text{Cu}^{2+}$  centers in CdS and in different polytypes of ZnS are summarized in Table II. The values of the crystal-field parameter  $Dq$  are not far from  $Dq=624$  (Ref. 2) and  $600 \text{ cm}^{-1}$  (Ref. 6) in the case of ZnS, and  $Dq=555 \text{ cm}^{-1}$  (Ref. 2) in the case of CdS reported above. The smaller values for CdS result from the larger interatomic distance in CdS compared with the ZnS crystal. It can be seen that the tetrahedral spin-orbit coupling parameters  $\zeta_{T_d}$  and  $\zeta'_{T_d}$  are nearly the same for all centers in ZnS, and are close to earlier fittings:  $\zeta = -593$  (Ref. 2) and  $-580 \text{ cm}^{-1}$ .<sup>6</sup> The comparison with the free-ion value of  $\zeta = -830 \text{ cm}^{-1}$  (Ref. 20) gives an estimate of the covalent bonding effect. The various centers differ in their trigonal spin-orbit coupling parameters  $\zeta_{C_{3v}}$  and  $\zeta'_{C_{3v}}$ . The energy of the local vibrational mode is practically the same for all the different centers in ZnS.

A comparison of the observed transitions in CdS (see Fig. 1) with the calculated energy-level scheme obtained from the fitting procedure is given in Table III. The comparison between the experimentally observed lines and the energy levels obtained from the fitting in case of the  $\text{Cu}^{2+}$  centers in ZnS polytypes is given in Table IV. In the case of the cubic AN center, we added the lowest calculated one-phonon line to the other so-called zero-phonon lines, deduced from the spin-orbit interaction of the  ${}^2T_2$  and  ${}^2E$  multiplets.

#### IV. ZEEMAN BEHAVIOR

The dependence of the energy levels on an external magnetic field  $\mathbf{B}$  is determined by supplementing the Hamiltonian Eq. (2) with the Zeeman operator, which in the simplest case and for tetrahedral symmetry has the form

$$H_Z = \mu_B (k\mathbf{l} + 2\mathbf{s}) \cdot \mathbf{B}. \quad (6)$$

Here  $\mathbf{l}$  and  $\mathbf{s}$  denote the orbital angular momentum and spin operators, respectively,  $\mu_B$  the Bohr magneton, and  $k$  the

TABLE VI. Comparison of the observed  $g$  factors of the cubic AN center of  $\text{Cu}^{2+}$  in ZnS with the calculated values. The magnetic-field-dependent  $g$  factors are calculated using Eq. (12) and the two limiting values for  $B=0 \text{ T}$  and  $B=20 \text{ T}$  are given. The zero-field energies are obtained from the fitting procedure and are given in meV.

Center	Multiplet	Energy	$g_{[-110]}^{\text{theor}}$	$g_{[-110]}^{\text{expt}}$	$g_{[111]}^{\text{theor}}$	$g_{[111]}^{\text{expt}}$
AN	$\Gamma_8({}^2E)$	858.46	1.68	$1.69 \pm 0.01$	1.57	$1.67 \pm 0.01$
			1.45		1.54	
	$\Gamma_8({}^2T_2)$	1.68	0.82–1.58	$0.96 \pm 0.15$	0.83–1.59	$0.96 \pm 0.15$
			2.28		2.25	
	$\Gamma_7({}^2T_2)$	0.00	0.79–0.43	$0.61 \pm 0.02$	0.79–0.44	$0.62 \pm 0.02$

TABLE VII. Comparison of the observed  $g$  factors of the axial centers AN1, AN2, AS, and PN of  $\text{Cu}^{2+}$  in ZnS with the calculated values. Energy levels  $\Gamma_{56}$  denote the Kramers doublet  $\Gamma_5\Gamma_6$ . The two theoretical  $g$  factors in brackets refer to the smallest and largest difference between the four energy levels of the  ${}^2E$  quartet. The magnetic-field-dependent  $g$  factors are given with respect to two limiting values  $B=0$  and 20 T or  $B=9$  and 20 T. For other explanations, see Table VI.

Multiplet	Energy	$g$ factors			
		$g_{\perp}^{\text{theor}}$	$g_{\perp}^{\text{expt}}$	$g_{\parallel}^{\text{theor}}$	$g_{\parallel}^{\text{expt}}$
AN1					
$\Gamma_{56}({}^2E)$	859.87	{1.34,1.60} <sup>a</sup>	$1.49 \pm 0.08$ <sup>a</sup>	1.68	$1.53 \pm 0.08$
$\Gamma_4({}^2E)$	859.77			1.65	$1.53 \pm 0.08$
$\Gamma_4({}^2T_2)$	2.26	0.94–0.58 <sup>b</sup>		0.9–0.6 <sup>c</sup>	
$\Gamma_{56}({}^2T_2)$	1.94	0.88–1.42 <sup>b</sup>		2.13	
$\Gamma_4({}^2T_2)$	0.00	0.75–0.49 <sup>c</sup>	$0.56 \pm 0.05$	1.0–0.7 <sup>c</sup>	$0.79 \pm 0.05$
AN2					
$\Gamma_{56}({}^2E)$	856.25	{1.34,1.61} <sup>a</sup>	$1.67 \pm 0.02$ <sup>a</sup>	1.65	$1.51 \pm 0.04$
$\Gamma_4({}^2E)$	856.04			1.61	$1.51 \pm 0.04$
$\Gamma_4({}^2T_2)$	2.25	0.93–0.57 <sup>b</sup>		1.0–0.7 <sup>c</sup>	
$\Gamma_{56}({}^2T_2)$	1.96	0.91–1.43 <sup>b</sup>		2.18	
$\Gamma_4({}^2T_2)$	0.00	0.7–0.4 <sup>c</sup>	$0.41 \pm 0.05$	1.1–0.8 <sup>c</sup>	$0.97 \pm 0.09$
AS					
$\Gamma_4({}^2E)$	859.62	{1.53,1.61} <sup>a</sup>	$1.64 \pm 0.02$ <sup>a</sup>	1.52	$1.45 \pm 0.02$
$\Gamma_{56}({}^2E)$	859.07			1.47	$1.45 \pm 0.02$
$\Gamma_4({}^2T_2)$	2.00	0.82–0.53 <sup>b</sup>		1.55–0.9 <sup>c</sup>	
$\Gamma_{56}({}^2T_2)$	1.88	1.09–1.50 <sup>b</sup>		2.45	
$\Gamma_4({}^2T_2)$	0.00	0.4–0.25 <sup>c</sup>	$0.29 \pm 0.02$	1.65–1.0 <sup>c</sup>	$1.45 \pm 0.02$
PN					
$\Gamma_{56}({}^2E)$	846.66	{1.11,1.71} <sup>a</sup>		1.68	
$\Gamma_4({}^2E)$	844.00		$0.00 \pm 0.02$	1.66	$1.71 \pm 0.02$
$\Gamma_4({}^2T_2)$	1.88	0.71–0.46 <sup>b</sup>		1.6–0.9 <sup>c</sup>	
$\Gamma_{56}({}^2T_2)$	1.82	1.20–1.57 <sup>b</sup>		2.38	
$\Gamma_4({}^2T_2)$	0.00	0.4–0.2 <sup>c</sup>	$0.28 \pm 0.03$	1.65–1.0 <sup>c</sup>	$1.35 \pm 0.05$

<sup>a</sup>Derived by taking the zero-field splitting and term interaction into account; see Eq. (11).

<sup>b</sup>Limiting values with respect to  $B=9$  and 20 T.

<sup>c</sup>Limiting values with respect to  $B=0$  and 20 T.

orbital reduction factor. In general the covalent bonding, described by the orbital reduction factor, may be different for different electronic wave functions of the excited quartet  $|{}^2E\nu\rangle$  and for the ground-state sextet  $|{}^2T_2\mu\rangle$  of the  $\text{Cu}^{2+}$  ion. Taking trigonal symmetry into account, the most general Zeeman matrix in the electronic subspace is made up of the matrices<sup>23</sup>

$$\langle \gamma | H_Z | \gamma' \rangle = \begin{pmatrix} A_1 & A_2 \\ A_2^+ & 0 \end{pmatrix} + 2\mu_B \langle \gamma | \mathbf{s} \cdot \mathbf{B} | \gamma' \rangle, \quad (7)$$

with

$$\begin{aligned} A_1 &= k_{\perp} \mu_B \langle {}^2T_2\mu | \frac{2}{3}C - \frac{1}{3}D | {}^2T_2\mu' \rangle \\ &\quad + k_{\parallel} \mu_B \langle {}^2T_2\mu | \frac{1}{3}C + \frac{1}{3}D | {}^2T_2\mu' \rangle, \\ A_2 &= k'_{\perp} \mu_B \langle {}^2T_2\mu | \frac{2}{3}C - \frac{1}{3}D | {}^2E\nu \rangle \\ &\quad + k'_{\parallel} \mu_B \langle {}^2T_2\mu | \frac{1}{3}C + \frac{1}{3}D | {}^2E\nu \rangle, \end{aligned} \quad (8)$$

and

$$C = \mathbf{l} \cdot \mathbf{B} = l_x B_x + l_y B_y + l_z B_z, \quad (9)$$

$$D = l_x B_y + l_y B_x + l_y B_z + l_z B_y + l_z B_x + l_x B_z.$$

The orbital reduction factors  $k_{\perp}$  and  $k_{\parallel}$  may be different depending on whether the Zeeman matrix is calculated using  ${}^2T_2$  wave functions ( $k_{\perp}, k_{\parallel}$ ) or a combination of  ${}^2T_2$  and  ${}^2E$  wave functions ( $k'_{\perp}, k'_{\parallel}$ ). In our description of Jahn-Teller active systems the orbital reduction factors describe covalent bonding effects with the impurity electronic  $d$  functions, and they are practically independent of an external magnetic field. We therefore introduced the following approximations, based on the values of the spin-orbit coupling parameters

$$k_{\perp} = \frac{\zeta_{\perp}}{\zeta_{fi}}, \quad k_{\parallel} = \frac{\zeta_{\parallel}}{\zeta_{fi}}, \quad k'_{\perp} = \frac{\zeta'_{\perp}}{\zeta_{fi}}, \quad k'_{\parallel} = \frac{\zeta'_{\parallel}}{\zeta_{fi}}, \quad (10)$$

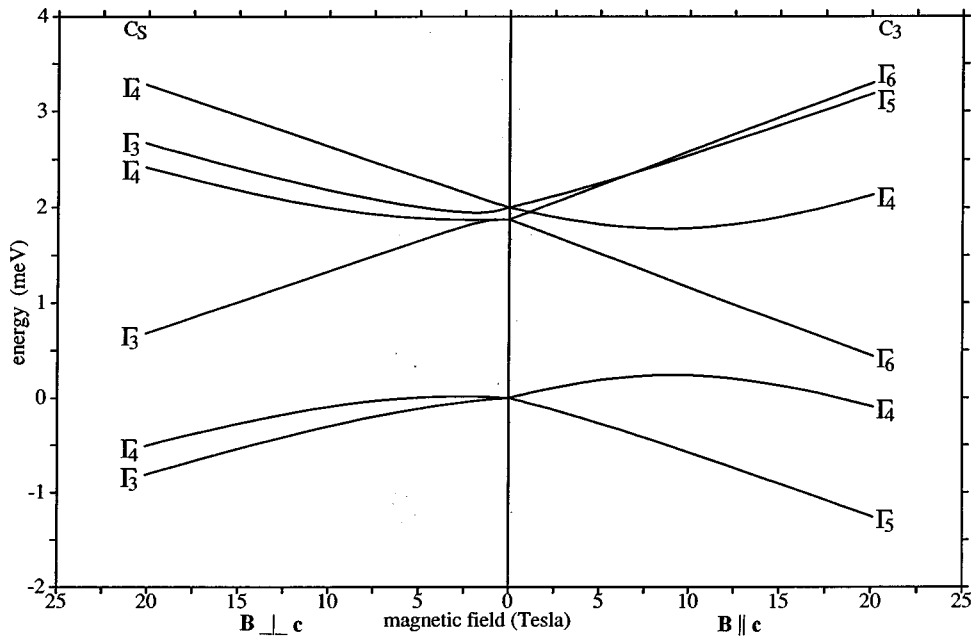


FIG. 5. Magnetic-field splitting of the  $\Gamma_4(^2T_2)$  ground state and the  $\Gamma_{56}(^2T_2)$  and  $\Gamma_4(^2T_2)$  doublets of the trigonal AS center calculated with  $N=8$ ; see text. The magnetic field is shown parallel to the  $c$  axis (right), and perpendicular to the  $c$  axis (left). Energies are given with respect to the zero-field ground state  $\Gamma_7(^2T_2)$ . Energy levels are assigned according to the irreducible representations of the corresponding symmetry double groups; see Table V.

where  $\zeta_{fi} = -830 \text{ cm}^{-1}$  is the value of the spin-orbit coupling parameter of the free  $\text{Cu}^{2+}$  ion.<sup>20</sup> Thus the orbital reduction factors  $k_{\perp}$ ,  $k_{\parallel}$ ,  $k'_{\perp}$ , and  $k'_{\parallel}$  are not taken as fitting parameters, but are considered to be determined entirely from the zero-field spectra. The orbital reduction factors then range from 0.55 to 0.97 for the different centers discussed. The use of Eq. (10) gives us the possibility of a parameter-free calculation of the magnetic-field splitting.

The experimentally observed magnetic-field splitting is often reported in terms of  $g$  factors,<sup>9-12</sup> even in cases where the splitting at low magnetic fields  $B$  could not be resolved. However, due to the repulsion of energy levels having the same symmetry, a nonlinear behavior of the lines is observed in many cases. To overcome this difficulty the nonlinear

splitting  $\Delta E(B)$  of two lines of the same symmetry, well separated from other lines of this symmetry, may be interpreted in terms of a zero-field splitting  $\Delta E(0)$  and a  $g$  factor according to<sup>27</sup>

$$\Delta E(B) = [\Delta E^2(0) + (\mu_B g B)^2]^{1/2}, \quad (11)$$

which approximately describes the term interaction of the two levels. This has been used in particular to interpret the observed nonlinear splitting  $\Delta E(B)$  of the excited  $^2E$  multiplet for  $\mathbf{B} \perp c$ .<sup>9</sup> Our calculation of the magnetic-field dependence of the lines, based on the fine-structure fit, may then also be used to derive the corresponding  $g$  factors from Eq. (11) to be compared with experiment. In the other cases the

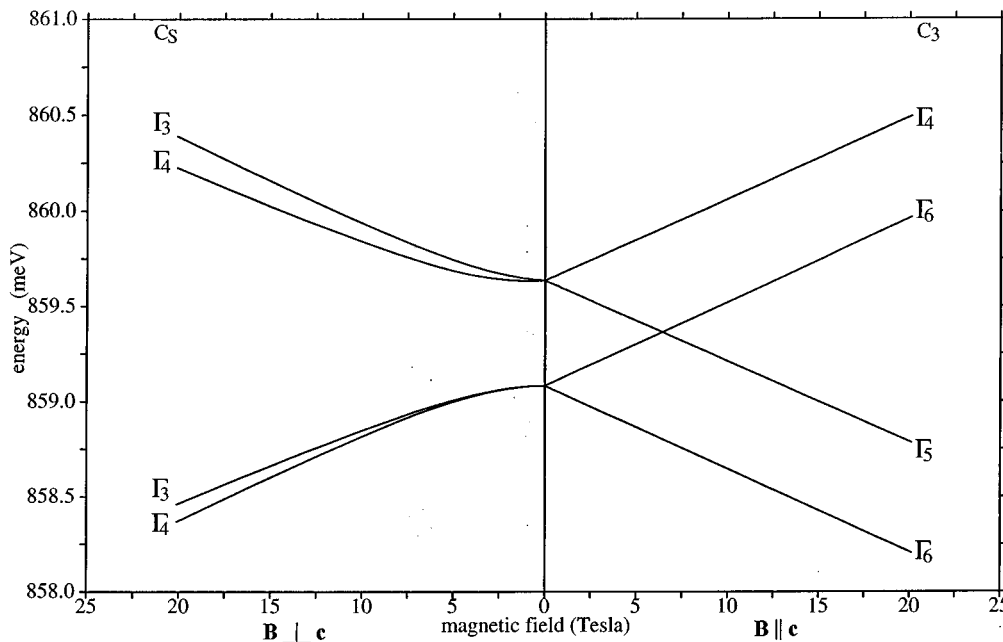


FIG. 6. Magnetic-field splitting of the excited lower  $\Gamma_{56}(^2E)$  and higher  $\Gamma_4(^2E)$  doublets of the trigonal AS center. Further explanations as in Fig. 5.

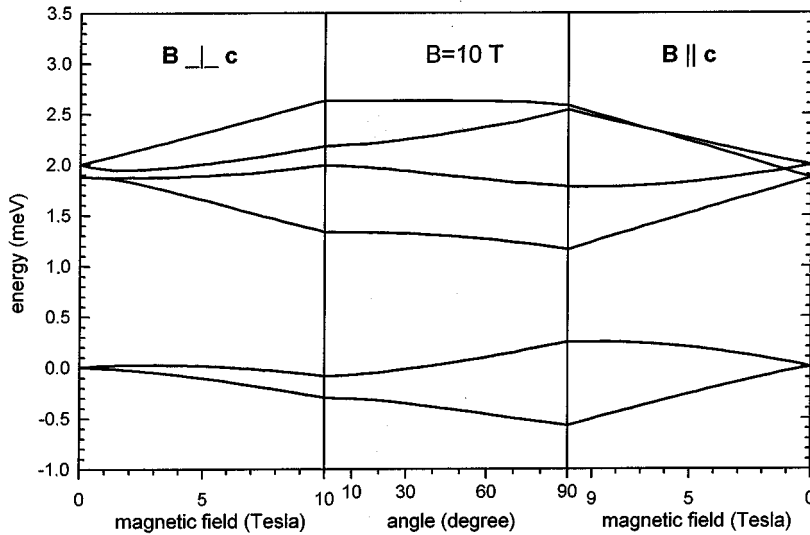


FIG. 7. Calculated angular magnetic-field splitting of the  $\Gamma_4(^2T_2)$  (lowest),  $\Gamma_{56}(^2T_2)$  (middle), and  $\Gamma_4(^2T_2)$  (highest) energy levels of the AS center in ZnS. The magnetic field is shown perpendicular to the  $c$  axis (left) and parallel to the  $c$  axis (right) as a function of the magnetic-field strength. The middle part shows the energy levels at  $B=10$  T as a function of the angle between  $\mathbf{B}$  and the  $c$  axis, varying from zero to  $90^\circ$ .

nonlinear magnetic-field dependence of the splitting  $\Delta E(B)$  may be described by a magnetic-field-dependent  $g$  factor defined by

$$g(B) = \frac{|\Delta E(B)|}{\mu_B B} \quad (12)$$

and a shift of the center of gravity of the two components.

The energy levels split because of the symmetry reduction from  $T_d$  to  $C_s$  or  $C_3$  symmetry for  $\mathbf{B}||[-110]$  and  $\mathbf{B}||[111]$ , respectively. In the case of  $C_{3v}$  the symmetry reduces to  $C_s$  or  $C_3$  for  $\mathbf{B}\perp[111]$  and  $\mathbf{B}||[111]$ , respectively. The energy levels are assigned according to one-dimensional irreducible representations  $\Gamma_4$ ,  $\Gamma_5$ , and  $\Gamma_6$  of the symmetry double group  $C_3$  or  $\Gamma_3$ ,  $\Gamma_4$  of  $C_s$ . The qualitative splitting is given in Table V.

The observed magnetic-field splitting of the optical transitions of various  $\text{Cu}^{2+}$  centers in ZnS are shown in Fig. 3. The assignments to the cubic AN center and the trigonal centers AN1, AN2, and AS are also given. The assignments  $\text{AS}_{\text{JT}}$  and  $\text{AN}_{\text{JT}}$  refer to the so-called Jahn-Teller transition at the AS and AN centers, respectively.

We start our discussion with the tetrahedral AN center of  $\text{Cu}^{2+}$  in ZnS. The observed splitting of the quartet AN in Fig. 3 is due to a twofold splitting of the excited  $\Gamma_8(^2E)$  and of the  $\Gamma_7(^2T_2)$  ground state. The nonlinear behavior can be described by a linear splitting with a  $g$  factor and a shift of the center of gravity. The corresponding  $g$  factors for the magnetic-field parallel to the  $[-110]$  and  $[111]$  directions are given in Table VI together with the theoretical values. The calculated splitting of the  $\Gamma_8(^2E)$  quartet confirms the splitting into two doublets, a higher  $\Gamma_4\Gamma_6$  and a lower  $\Gamma_3\Gamma_6$  of  $C_3$  in the case of  $\mathbf{B}||[111]$  and two  $\Gamma_3\Gamma_4$  doublets of  $C_s$  in case of  $\mathbf{B}||[-110]$ ; see Table V. The calculated  $g$  factors are compatible with the observation; see Table VI.

The theoretical splittings of the  $\Gamma_7(^2T_2)$  ground-state doublet and the  $\Gamma_8(^2T_2)$  quartet are shown in Fig. 4. The assignments of the energy levels are according to the different irreducible representations of the symmetry double groups  $C_s$  and  $C_3$ ; see Table V. The splitting is clearly nonlinear except for the two  $\Gamma_6$  levels of the  $\Gamma_8(^2T_2)$  quartet.

The reason for this is the small energetic difference between both multiplets for  $B=0$ , leading to a repulsion of energy levels having the same symmetry. The nonlinear behavior of the energy levels originating from the  $\Gamma_7(^2T_2)$  ground state may be described by a shift of the center of gravity for the  $\Gamma_4$  and  $\Gamma_5$  components, which is 0.42 meV downwards at  $B=15$  T. This has to be compared with the observed shift of the two nonlinear components of the AN quartet of 0.21 meV in Fig. 3. The calculated energetic splitting of the  $\Gamma_7(^2T_2)$  ground state, using Eq. (12), leads to a magnetic-field-dependent  $g$  factor. Therefore, in Table VI we give the two limiting values for  $B=0$  and 20 T. The experimentally observed  $g$  factors lie within this region, and agree with theory for  $B=11$  T.

The transition between the  $\Gamma_8(^2E)$  and  $\Gamma_8(^2T_2)$  multiplets at 856.78 meV, which is observed in emission only, was discussed controversially in the literature.<sup>4-6</sup> According to Ref. 9 the observed splitting of this Jahn-Teller emission with  $g=0.96$  (see Table VI) is assigned in agreement with Clerjaud and Gelineau<sup>5</sup> to the splitting of the  $\Gamma_8(^2T_2)$  ground state. It must be emphasized, however, that our fitting procedure yields a moderate Jahn-Teller coupling with a Huang-Rhys factor of  $S=0.81$ , in contrast to Ref. 5, where a rather strong Jahn-Teller coupling with  $S=3$  was used. Our calculations give an unambiguous fourfold splitting of the  $\Gamma_8(^2T_2)$  quartet; see Fig. 4. The splitting of the two  $\Gamma_6$  components result in a  $g$  factor of 2.25, and the splitting of the  $\Gamma_4$  and  $\Gamma_5$  components give a  $g$  factor between 0.8 and 0.4 for  $B=0$  and 20 T, respectively. This has to be compared with the observed value of  $g=0.96$ ; see Table VI. It might therefore be possible that the observed splitting of the  $\Gamma_8(^2T_2)$  quartet is due to the energetic difference between the lowest  $\Gamma_6$  and the  $\Gamma_4$  level for which the  $g$  factor vary between  $g=0.82$  at  $B=0$  T and  $g=1.58$  at  $B=20$  T; see Table VI. Our calculations reproduce the observed  $g$  factor approximately at a magnetic field of  $B=6$  T. We therefore conclude that our results are in agreement with the measurements (see Fig. 3), and support this interpretation of the Jahn-Teller emission.

The trigonal centers AN1, AN2, AS, and PN in ZnS crystals exemplify the symmetry lowering of the  $\text{Cu}^{2+}$  environ-

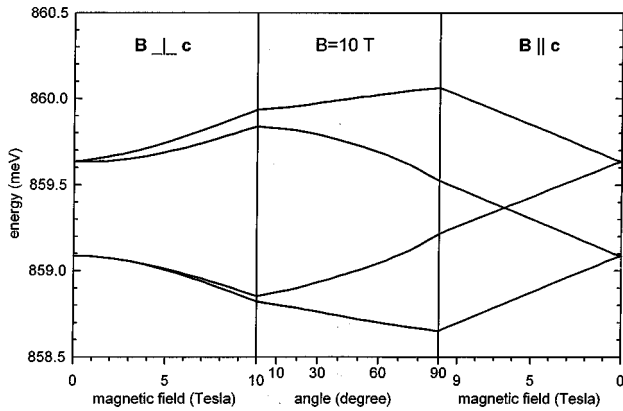


FIG. 8. Calculated angular magnetic-field splitting of the excited  ${}^2E$  energy levels of the AS center in  $\text{ZnS}$ . Explanations are the same as in Fig. 7.

ment due to different crystalline polytypes. The deviation from tetrahedral symmetry is described by the comparatively small parameters  $K$ ,  $K'$ ,  $\zeta_{C_{3v}}$ , and  $\zeta'_{C_{3v}}$ . The Zeeman patterns are characterized by the zero-field splitting of the transition lines at 0.86 eV,<sup>17</sup> which is due to the splitting of the  $\Gamma_8({}^2E)$  quartet under the  $C_{3v}$  symmetry double group into a doublet  $\Gamma_4({}^2E)$  and a Kramers doublet  $\Gamma_{56}({}^2E)$ ; see Table VII. The Jahn-Teller emission of the cubic AN center at 856.78 meV splits into a lower  $\Gamma_{56}({}^2T_2)$  and a higher  $\Gamma_4({}^2T_2)$ , and the emission from the  $\Gamma_{56}({}^2E)$  to the  $\Gamma_{56}({}^2T_2)$  level has been established for the AS and PN centers, but no  $g$  factors or zero-field splittings have been reported so far. In connection with this splitting of the  ${}^2T_2$  ground state, it could be shown that the so called Jahn-Teller emission zero-phonon lines, which are observed in emission only, are a general phenomenon of the  $\text{Cu}^{2+}$  center in sulfide compounds.

As an example of the trigonal centers of  $\text{Cu}^{2+}$  in  $\text{ZnS}$ , Fig. 5 shows the calculated Zeeman splitting of the lowest  $\Gamma_4({}^2T_2)$  doublet, the Kramers doublet  $\Gamma_{56}({}^2T_2)$ , and of the highest  $\Gamma_4({}^2T_2)$  doublet of the ground state  ${}^2T_2$  for the AS center. Figure 6 shows the Zeeman splitting of the excited

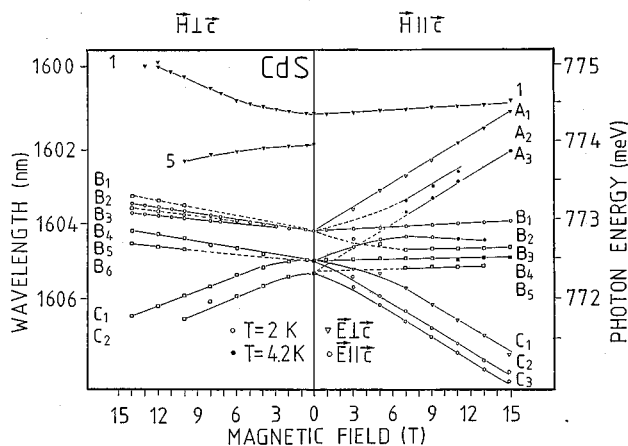


FIG. 9. Magnetic-field splitting of the fine-structure optical transitions of the  $\text{Cu}^{2+}$  center in  $\text{CdS}$  for magnetic fields perpendicular (left) and parallel (right) to the  $c$  axis.

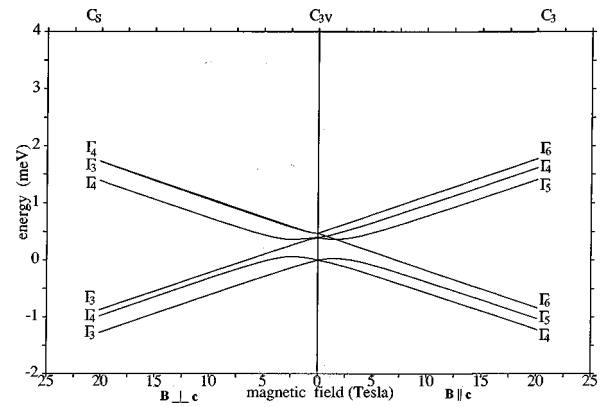


FIG. 10. Calculated magnetic-field splitting of the  $\Gamma_4({}^2T_2)$  ground state and the  $\Gamma_4({}^2T_2)$  (middle) and  $\Gamma_{56}({}^2T_2)$  (highest) quartets of the  $\text{Cu}^{2+}$  center in  $\text{CdS}$ . Explanations are the same as in Fig. 5.

$\Gamma_{56}({}^2E)$  Kramers doublet and the  $\Gamma_4({}^2E)$  doublet for the same center. These Zeeman patterns show a clearly anisotropic behavior, and are representative of all axial centers observed in  $\text{ZnS}$ , except for the reversed fine-structure splitting of the excited  ${}^2E$  quartet; see the negative value of the parameter  $D_0$  in Table II. In the case of  $\mathbf{B}\parallel\mathbf{c}$  the splitting of the  $\Gamma_4({}^2E)$  and  $\Gamma_{56}({}^2E)$  excited states is linear with respect to the magnetic field; see Fig. 6. This is a consequence of the different symmetries of the nearby components of the trigonal crystal-field splitting, which do not allow for a term interaction.

The calculated magnetic-field splittings of the axial centers AN1, AN2, AS, and PN in terms of  $g$  factors are compared with the experimental values in Table VII. The nonlinear splittings of the  $\Gamma_4({}^2T_2)$  ground state and the  $\Gamma_{56}({}^2T_2)$  and  $\Gamma_4({}^2T_2)$  doublets are described by magnetic-field-dependent  $g$  factors using Eq. (12), and Table VII gives the two limiting values for  $B=0$  or 9 T, and  $B=20$  T. The  ${}^2E$  excited quartet is split by the magnetic field into four lines showing a small zero-field splitting; however, in the case of  $\mathbf{B}\perp\mathbf{c}$  only two lines are observed. We evaluated the  $g$  factors using Eq. (11), and the mean value of the two calculated ones may be compared with the single measured value.

In the case of  $\mathbf{B}\parallel\mathbf{c}$  the calculated  $g$  factors of the  $\Gamma_4({}^2T_2)$  ground state vary with respect to the magnetic field, whereas the observed splitting is linear. The magnitudes of the splitting, however, are quite compatible. There are slight differences between the observed and calculated  $g$  factors for the excited  $\Gamma_4({}^2E)$  and  $\Gamma_{56}({}^2E)$  doublets, but the general feature of the Zeeman pattern is explained. In the cases of  $\Gamma_{56}({}^2T_2)$  and  $\Gamma_4({}^2T_2)$  higher doublets, the splitting is similar to the splitting of the  $\Gamma_8({}^2T_2)$  quartet of the cubic AN center. In Table VII we give the large  $g$  factor of the two  $\Gamma_6$  components, which are split linearly, and the varying  $g$  factor with respect to the  $\Gamma_4$  and  $\Gamma_5$  components according to Table V. The situation is different, however, for  $\mathbf{B}\perp\mathbf{c}$ , where two energy levels of  $\Gamma_3$  or  $\Gamma_4$  symmetry come close together. This leads to a strong nonlinear behavior for small magnetic fields below 5 T. Therefore, in Table VII we give two limiting values of the  $g$  factors at  $B=9$  and 20 T for the nearby multiplets  $\Gamma_{56}({}^2T_2)$  and  $\Gamma_4({}^2T_2)$  using Eq. (12). The reason for this is that the calculation shows that the observed

TABLE VIII. Comparison of the observed  $g$  factors of  $\text{Cu}^{2+}$  in CdS with the calculated values. The experimental  $g$  factors have been deduced for magnetic fields between  $B=7$  and 15 T. The theoretical magnetic-field-dependent  $g$  factors are given for the two limiting values  $B=7$  and 20 T. Energies are given in meV.

Multiplet	Energy	$g_{\perp}^{\text{theor}}$	$g_{\perp}^{\text{expt}}$	$g_{\parallel}^{\text{theor}}$	$g_{\parallel}^{\text{expt}}$
$\Gamma_{56}(^2E)$	774.40	0.01–0.03	$0.00 \pm 0.05$	1.56	$1.55 \pm 0.02$
$\Gamma_4(^2E)$	772.88	0.16–0.15	$0.09 \pm 0.03$	1.55	$1.55 \pm 0.02$
$\Gamma_{56}(^2T_2)$	0.56	0.1–0.0		2.23	$1.70 \pm 0.10$
$\Gamma_4(^2T_2)$	0.41	1.4–1.95	$1.15 \pm 0.05$	2.43–2.26	$1.87 \pm 0.02$
$\Gamma_4(^2T_2)$	0.00	0.6–0.3	$0.13 \pm 0.03$	2.43–2.26	$1.93 \pm 0.02$

$g_{\perp}$  factor for the  $\Gamma_4(^2T_2)$  ground state is reproduced in the region between 9 and 20 T. In the case of the AS center the nonlinear splitting of the  $\Gamma_4(^2T_2)$  ground state for  $\mathbf{B} \perp \mathbf{c}$  results in a calculated  $g$  factor at  $B=15$  T of  $g_{\perp}=0.31$ , which is close to the observed behavior; see Table VII. The calculated splitting of the excited  $\Gamma_{56}(^2E)$  and  $\Gamma_4(^2E)$  doublets in the case of  $\mathbf{B} \perp \mathbf{c}$  (see Fig. 6) is evaluated using Eq. (11), thus giving two close  $g$  factors, referring to the smallest and largest differences between the four energy levels of the  $^2E$  quartet. This is done because only one  $g$  factor has been resolved in the experiment, which has been deduced with the help of Eq. (11) and may be compared with the mean value of the calculated  $g$  factors, which is 1.57 in the case of the AS center. The sequence of energy levels of the  $^2T_2$  multiplet with respect to their symmetry of the  $C_s$  double group cannot completely be determined from the observed polarizations and selection rules, but are given from the calculated splittings. Therefore, we find agreement between the observed and calculated Zeeman splittings in the case of the AS center; see Table VII.

The situation is not very different for the other trigonal  $\text{Cu}^{2+}$  centers in ZnS. The calculated splittings of the three doublets  $\Gamma_4(^2T_2)$  (ground state),  $\Gamma_{56}(^2T_2)$ , and  $\Gamma_4(^2T_2)$  show a nonlinear behavior in the  $\mathbf{B} \perp \mathbf{c}$  configuration for all trigonal centers in ZnS. The experimentally observed  $g$  factors are in all cases within the region of the variation of the calculated  $g$  factors between  $B=9$  and 20 T; see Table VII. There are no reported  $g_{\perp}$  values for the  $\Gamma_{56}(^2T_2)$  Kramers doublet, though the emission lines were observed for the AS and PN centers at 1.88 and 1.82 meV above the ground state, respectively.<sup>9</sup> There are no observed transitions to the nearby  $\Gamma_4(^2T_2)$  doublet of the four centers, and the calculated magnetic-field-dependent  $g$  factors for  $\mathbf{B} \perp \mathbf{c}$  are given for both doublets in Table VII in the region between  $B=9$  and 20 T for the same reason as before. The calculation shows a strong nonlinear behavior for small magnetic fields below  $B=5$  T as a consequence of the term interaction of the two  $\Gamma_3$  states or the two  $\Gamma_4$  states. In the case of  $\mathbf{B} \parallel \mathbf{c}$  the splittings of the  $\Gamma_4(^2T_2)$  ground state and of the other  $\Gamma_4(^2T_2)$  state are nonlinear, and the magnetic-field-dependent  $g$  factors are given in Table VII in terms of the two limiting values for  $B=0$  and 20 T. The  $\Gamma_{56}(^2T_2)$  Kramers doublets show a linear splitting for  $\mathbf{B} \parallel \mathbf{c}$ , as can be seen from Fig. 5 in the case of the AS center, but no  $g$  factors are observed for the trigonal centers.

The angular dependence of the magnetic-field splitting of the  $^2T_2$  energy levels of the AS center is shown in Fig. 7 as an example of the trigonal  $\text{Cu}^{2+}$  centers in ZnS. The middle

part shows the energy levels as a function of the angle between the magnetic field and the  $c$  axis at a magnetic field of  $B=10$  T. The calculation has been done taking  $N=8$  excited energy levels of the local vibrational mode into account. Figure 8 shows the corresponding splittings of the lower  $\Gamma_{56}(^2E)$  Kramers doublet and the higher  $\Gamma_4(^2E)$  doublet of the excited  $^2E$  multiplet. The figure illustrates the different splittings of the two doublets of  $C_{3v}$  symmetry for different directions of the magnetic field with respect to the  $c$  axis. One can see that the definitions of a  $g$  factor from the splitting of a degenerate energy level is different for  $\mathbf{B} \perp \mathbf{c}$  and  $\mathbf{B} \parallel \mathbf{c}$  in the sense that one and the same energy level may belong to different zero-field states when the direction of the magnetic field changes. The same may be seen from Fig. 7 for the  $\Gamma_{56}(^2T_2)$  Kramers doublet and the higher  $\Gamma_4(^2T_2)$  doublet.

We now turn to the  $\text{Cu}^{2+}$  center in CdS crystals. The experimentally observed fine-structure splittings are shown in Fig. 9 after Ref. 10. It shows the experimentally observed emission lines emerging from the allowed transitions between the excited  $^2E$  states and the  $^2T_2$  ground states. The transitions at zero magnetic field are assigned to lines 1 (highest), 5, 2, 3, and 4; see Fig. 1. The magnetic-field splitting is approximately linear above  $B=7$  T, and the corresponding  $g$  factors, taken from the region  $7 \text{ T} \leq B \leq 15 \text{ T}$ , are compiled in Table VIII for magnetic fields parallel and perpendicular to the  $c$  axis. The calculated Zeeman splittings of the  $^2T_2$  ground state and the  $^2E$  excited state are shown in Figs. 10 and 11. The calculations were done taking  $N=9$  excited states of the local vibrational mode into account. Comparing with Fig. 9, it can be seen that the observed general nonlinear behavior of the splittings is reproduced by the calculation. In order to compare the theoretical results with the observed splittings it is necessary to determine the symmetry of the initial and final states of the various transitions from the polarization of the observed lines and the selection rules. This had been done with the help of the calculated splittings, and the comparison between the observed and calculated  $g$  factors is shown in Table VIII.

The experimental  $g$  factors are deduced from the region  $7 \text{ T} \leq B \leq 15 \text{ T}$ . In order to compare with the observation, in Table VIII we give the two limiting values of the calculated magnetic-field-dependent  $g$  factors for the two limiting fields  $B=7$  and 20 T. The splitting of the excited-state doublets  $\Gamma_4(^2E)$  and  $\Gamma_{56}(^2E)$  is reproduced by the calculation. In particular, the calculated splitting of the lower  $\Gamma_4(^2E)$  doublet for  $\mathbf{B} \perp \mathbf{c}$  confirms the small observed splitting, the  $g$  factor of which was difficult to deduce from the experiments.

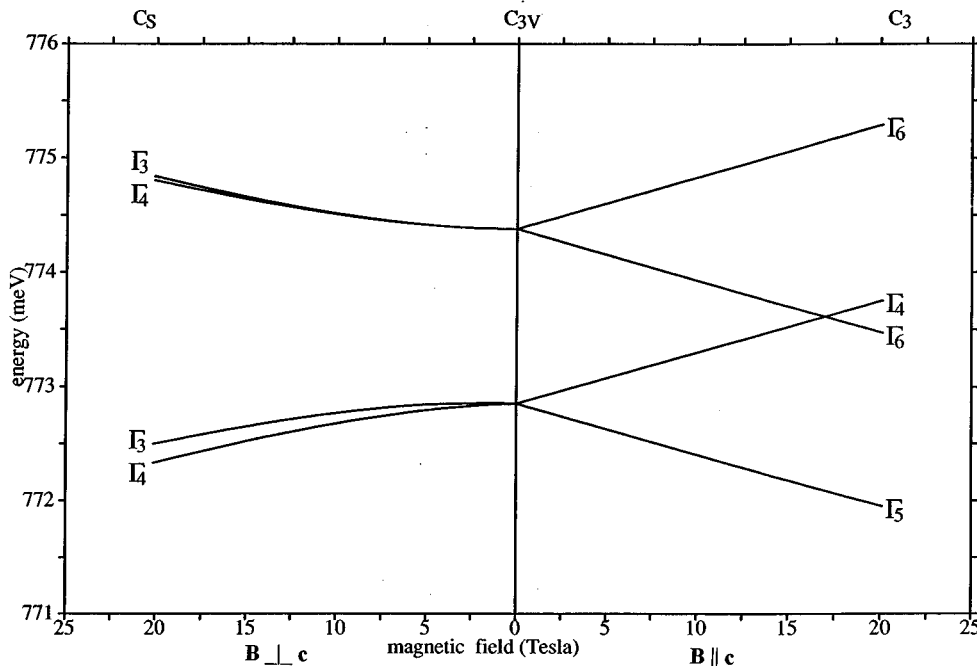


FIG. 11. Calculated magnetic-field splittings of the excited lower  $\Gamma_4(^2E)$  doublet and higher  $\Gamma_{56}(^2E)$  Kramers doublet of the  $\text{Cu}^{2+}$  center in  $\text{CdS}$ . Explanations are the same as in Fig. 5.

There are, however, some discrepancies between the observed and calculated  $g$  factors of the three doublets of the  $^2T_2$  ground state, since the calculated  $g$  factors for  $\mathbf{B} \parallel \mathbf{c}$  and for  $\mathbf{B} \perp \mathbf{c}$  are generally larger than the observed ones; see Table VIII. This is a striking difference from the situation in  $\text{ZnS}$ , where a general agreement between the experimental data and the calculation was achieved. This may be due to the neglect of the Jahn-Teller coupling to a local vibrational mode of  $T_2$  symmetry. A local vibrational mode of  $T_2$  symmetry is at about 20.8 meV in the phonon-energy gap of  $\text{CdS}$ , whereas a hybridization with the acoustic band occurs in  $\text{ZnS}$ .

## V. DISCUSSION

The correct interpretation of the fine structure, i.e., the correctness of the fitted parameters, is demonstrated by the parameter-free calculations of the magnetic-field splittings in case of the various  $\text{Cu}^{2+}$  centers in  $\text{ZnS}$ . The magnetic-field splitting depends sensitively on the wave functions, which are calculated from the fitting procedure of the fine structure. In addition, the nonlinear behavior of the transition lines with respect to the magnetic field is due to the term interaction between states of the same symmetry. This term interaction depends on the wave functions and the relative energetic differences of the corresponding energy levels. The nonlinear behavior is therefore decisive for an understanding of the observed spectra.

The agreement between calculated and observed magnetic-field-dependent transitions is not so striking for the  $\text{Cu}^{2+}$  center in  $\text{CdS}$  as it is for  $\text{ZnS}$ . The reason for this is the stronger nonlinear behavior of the energy levels of the ground state  $^2T_2$  compared with experiment. We believe that this is due to the fact that copper centers in  $\text{CdS}$  for a local vibrational mode of  $T_2$  symmetry at 20.8 meV in the phonon-energy gap,<sup>21</sup> so that the Jahn-Teller coupling to this mode should not be neglected. This could be clarified by a

calculation of a two-mode coupling, where a local vibrational mode of  $T_2$  symmetry together with the coupling to an  $E$  mode is taken into account. However, for a perfect understanding of the observed optical transitions, more information is necessary on the Jahn-Teller effect, and especially on the local vibrational modes involved. It must be noted that the very indirect way of determining the energy and symmetry of the local vibrational mode from the observed optical fine-structure transitions leads to an uncertainty, which depends on the number of lines observed. An independent and unambiguous determination of the local vibrational mode at the copper defect in different crystalline environments would remove this uncertainty, and would help to find the correct interpretation of the spectra. The energy and symmetry of the local vibrational modes can in principle be determined from Raman-scattering experiments.

Our method discussed here leads to a qualitative understanding not only of the fine structure of the optical transitions but also of the magnetic-field splittings. In addition, a numerical agreement between observed and calculated  $g$  factors has been achieved for most of the energy levels. The observed nonlinear behavior with respect to the magnetic field could be understood from the calculations, which also gave the symmetry of the various energy levels. For a direct comparison between the observed and calculated Zeeman lines, see Ref. 28.

In summary, it is a striking fact that the simple coupling to an  $E$  mode explains the fine structure and the general Zeeman behavior of the  $\text{Cu}^{2+}$  centers in  $\text{ZnS}$  and  $\text{CdS}$ .

## ACKNOWLEDGMENTS

The authors are grateful to J. Schöpp and C. Schrepel for valuable discussions and a critical reading of the manuscript. We thank the Zentraleinrichtung Rechenzentrum of the Technische Universität Berlin and the Konrad-Zuse-Zentrum für Informationstechnik Berlin for their support and the provision of computing facilities.

- <sup>1</sup>H. A. Weakliem, *J. Chem. Phys.* **36**, 2117 (1962).
- <sup>2</sup>I. Broser, H. Maier, and H. -J. Schulz, *Phys. Rev.* **140**, 2135 (1965).
- <sup>3</sup>M. De Wit, *Phys. Rev.* **177**, 441 (1969).
- <sup>4</sup>I. Broser, U. Scherz, and M. Wöhlecke, *J. Lumin.* **1**, 39 (1970).
- <sup>5</sup>B. Clerjaud and A. Gelineau, *Phys. Rev. B* **9**, 2832 (1974).
- <sup>6</sup>H. Maier and U. Scherz, *Phys. Status Solidi B* **62**, 153 (1974).
- <sup>7</sup>U. Sauer, U. Scherz, and H. Maier, *Phys. Status Solidi B* **62**, K71 (1974).
- <sup>8</sup>C. M. Weinert and U. Scherz, *Phys. Status Solidi B* **124**, 287 (1984).
- <sup>9</sup>P. Thurian, Ph.D. thesis, Technische Universität Berlin, Köster-Verlag, 1994.
- <sup>10</sup>A. Hoffmann, I. Broser, P. Thurian, and R. Heitz, *J. Cryst. Growth* **101**, 532 (1990).
- <sup>11</sup>I. Broser, A. Hoffmann, R. Heitz, and P. Thurian, *J. Lumin.* **48&49**, 693 (1991).
- <sup>12</sup>P. Thurian, R. Heitz, T. Jentsch, A. Hoffmann, and I. Broser, *Physica B* **185**, 239 (1993).
- <sup>13</sup>J. Schöpp, Ph.D. thesis, Technische Universität Berlin, 1992.
- <sup>14</sup>J. Schöpp, R. Heitz, A. Hoffmann, and U. Scherz, *Mater. Sci. Forum* **143-147**, 815 (1994).
- <sup>15</sup>I. Broser and R. Broser-Warminsky, *Dtsch. Patentamt*, Patent No. **814**, 193 (1950).
- <sup>16</sup>T. Buch, B. Clerjaud, B. Lambert, and P. Kovacs, *Phys. Rev. B* **7**, 184 (1973).
- <sup>17</sup>U. W. Pohl, A. Ostermeier, W. Busse, and H. E. Gumlich, *Phys. Rev. B* **42**, 5751 (1990).
- <sup>18</sup>R. Heitz, A. Hoffmann, P. Thurian, and I. Broser, *J. Phys. C* **4**, 157 (1992).
- <sup>19</sup>U. Scherz, *J. Phys. Chem. Solids* **30**, 2077 (1969).
- <sup>20</sup>R. E. Dietz, H. Kamimura, M. D. Sturge, and A. Yariv, *Phys. Rev.* **132**, 1559 (1963).
- <sup>21</sup>T. Yamaguchi and H. Kamimura, *J. Phys. Soc. Jpn.* **33**, 953 (1972).
- <sup>22</sup>G. Kaczmarczyk, R. Heitz, P. Thurian, A. Hoffmann, I. Broser, and U. Scherz (unpublished).
- <sup>23</sup>T. Telahun, Ph.D. thesis, Technische Universität Berlin, Köster-Verlag, 1994.
- <sup>24</sup>J. S. Griffith, *The Theory of Transition-Metal Ions* (Cambridge University Press, Cambridge, 1971).
- <sup>25</sup>Wykoff, *Crystal Structures* (Wiley, New York, 1963).
- <sup>26</sup>P. Koidl, O. F. Schirmer, and U. Kaufmann, *Phys. Rev. B* **8**, 4926 (1973).
- <sup>27</sup>R. M. MacFarlane, *Phys. Rev. B* **1**, 989 (1970).
- <sup>28</sup>T. Telahun, P. Thurian, A. Hoffmann, I. Broser, and U. Scherz, *Mater. Sci. Forum* (to be published).